Evaluating atmospheric CO_2 inversions at multiple scales over a highly inventoried agricultural landscape

ANDREW E. SCHUH*†, THOMAS LAUVAUX‡, TRISTRAM O. WEST§, A. SCOTT DENNING¶, KENNETH J. DAVIS‡, NATASHA MILES‡, SCOTT RICHARDSON‡, MAREK ULIASZ¶, ERANDATHIE LOKUPITIYA∥, DANIEL COOLEY**, ARLYN ANDREWS†† and STEPHEN OGLE†

*Cooperative Institute for Research in the Atmosphere, Colorado State University, Fort Collins, CO, USA, †Natural Resources Ecology Laboratory, Colorado State University, Fort Collins, CO, USA, ‡Department of Meteorology, Pennsylvania State University, University Park, PA, USA, §Joint Global Change Research Institute, Pacific Northwest National Laboratory, College Park, MD, USA, ¶Department of Atmospheric Sciences, Colorado State University, Fort Collins, CO, USA, ∥Department of Zoology, University of Colombo, Colombo 03, Sri Lanka, **Department of Statistics, Colorado State University, Fort Collins, CO, USA, ††NOAA Earth System Research Laboratory, Boulder, CO, USA

Abstract

An intensive regional research campaign was conducted by the North American Carbon Program (NACP) in 2007 to study the carbon cycle of the highly productive agricultural regions of the Midwestern United States. Forty-five different associated projects were conducted across five US agencies over the course of nearly a decade involving hundreds of researchers. One of the primary objectives of the intensive campaign was to investigate the ability of atmospheric inversion techniques to use highly calibrated CO_2 mixing ratio data to estimate CO_2 flux over the major croplands of the United States by comparing the results to an inventory of CO_2 fluxes. Statistics from densely monitored crop production, consisting primarily of corn and soybeans, provided the backbone of a well studied bottom-up inventory flux estimate that was used to evaluate the atmospheric inversion results. Estimates were compared to the inventory from three different inversion systems, representing spatial scales varying from high resolution mesoscale (PSU), to continental (CSU) and global (CarbonTracker), coupled to different transport models and optimization techniques. The inversion-based mean CO_2-C sink estimates were generally slightly larger, 8–20% for PSU, 10–20% for CSU, and 21% for CarbonTracker, but statistically indistinguishable, from the inventory estimate of 135 TgC. While the comparisons show that the MCI region-wide C sink is robust across inversion system and spatial scale, only the continental and mesoscale inversions were able to reproduce the spatial patterns within the region. In general, the results demonstrate that inversions can recover CO_2 fluxes at sub-regional scales with a relatively high density of CO_2 observations and adequate information on atmospheric transport in the region.

Keywords: agriculture, atmospheric inversions, carbon cycle, CO_2 emissions, inventory, Mid-Continent Intensive

Received 6 November 2012; revised version received 6 November 2012 and accepted 10 December 2012

Introduction

For over half a century, the analysis of trace gases in the atmosphere has been a rich source of information about the contemporary global carbon cycle. Early studies of the secular trend and seasonal cycles of CO_2 mixing ratio revealed the accumulation of fossil carbon and the striking role of terrestrial ecosystems in planetary metabolism, and by the mid-1960s scientists had used spatial patterns in CO_2 and its isotopic composition to establish rates of atmospheric mixing (Bolin & Erickson, 1959; Bolin & Keeling, 1963), the penetration of anthropogenic CO_2 into the oceans, and the existence of a net sink in the terrestrial biosphere (Bolin & Keeling, 1963). Beginning in the 1980s, the global network of sampling stations from which accurate CO_2 measurements were available expanded rapidly with CO_2 measurements to support carbon cycle research. Denser data allowed formal estimation of the spatial patterns of sources and sinks at continental and ocean basin scale using inverse modeling, which also required quantitative accounting for atmospheric transport (Pearman & Hyson, 1981; Heimann & Keeling, 1986; Fung *et al.*, 1987; Tans *et al.*, 1990). A community of global CO_2 inverse modelers emerged during the 1990s and performed a series of atmospheric transport intercomparison (TransCom) experiments. TransCom

Correspondence: Andrew E. Schuh, tel. + 970 491 8362, fax + 970 491 8449, e-mail: aschuh@atmos.colostate.edu

documented the sensitivity of estimated source/sink patterns to differences in advection, turbulence, and cloud transport among atmospheric models (Law & Simmonds, 1996; Denning *et al.*, 1999; Gurney *et al.*, 2002; Baker *et al.*, 2006).

Despite decades of measurements, modeling, and field experiments, interactions between the carbon cycle, climate, and management now constitute a leading source of uncertainty in projections of 21st century climate change. Experiments with fully coupled carbon cycle-climate models show a range of over 250 ppm in CO_2 by 2100 given identical fossil fuel emissions (Friedlingstein *et al.*, 2006; Solomon *et al.*, 2007). Estimation of space/time variations of carbon sources and sinks by transport inversion provide an important constraint on coupled Earth system prediction. Tracking interannual variations in carbon source and sinks using transport inversion of atmospheric observation has become nearly routine in the 21st century (Peters *et al.*, 2007, 2010). However, the relatively sparse data still require aggressive regularization through the use of Bayesian priors (Baker *et al.*, 2006), geospatial smoothing (Michalak *et al.*, 2004), or pre-aggregation of sources and sinks into coarse basis functions within which space/time patterns of flux are assumed to be known (Peters *et al.*, 2007).

Formal evaluation of the accuracy of regional sources and sinks has remained elusive due to a lack of reliable independent measurements of regional CO_2 fluxes. CO_2 fluxes can be estimated locally by eddy covariance (Baldocchi *et al.*, 2012), but the area represented by these estimates is generally a few square kilometers at maximum, far smaller than can be estimated from available concentration data. Field experiments during which greatly enhanced data collection is performed temporarily over a limited region and time period has provided opportunities to evaluate transport inversions (RECAB: Filippi *et al.*, 2003; ChEAS: http://cheas.p-su.edu/Chen *et al.*, 2008; LBA: http://daac.ornl.gov/LBA/lba.shtml, COBRA: Gerbig *et al.*, 2003; CERES: Dolman *et al.*, 2006; ORCA: Goeckede *et al.*, 2010a; ACME-07: Desai *et al.*, 2011). Even for such limited regions, local bottom-up flux products (estimated from surface data, in contrast to models) must be interpolated across orders of magnitude of spatial scales to provide a quantitative constraint on top-down fluxes (estimated from atmosphere measurements).

As part of the North American Carbon Program (NACP) (Wofsy & Harriss, 2002; Denning, 2005), the Mid-Continent Intensive (MCI) field experiment was designed to evaluate innovative methods for CO_2 flux inversion and data assimilation by performing quantitative comparison of top-down and bottom-up inventory estimates of a regional carbon budget. The experiment was performed over a relatively flat, heavily managed landscape in the mid-continent region of North America and featured a high density of atmospheric CO_2 measurements (Ogle *et al.*, 2006). A significant advantage of the study region was the fact that this area was relatively flat and devoid of complex topography, that would have made the meteorology more difficult to model for the inversions. Atmospheric CO_2 concentrations were measured using *in situ* analyzers installed on a ring of communication towers in the region (Miles *et al.*, 2012), and vertical profiles of CO_2 were measured by a short dense aircraft sampling campaign (Martins *et al.*, 2009). Another key advantage of this region for the inventory compilation was the detailed statistics available from US Department of Agriculture on commodity production in this economically important region. Consequently, the bottom-up inventory was developed at a high spatial resolution compared to previous studies and provided highly resolved maps of the annual uptake and release of CO_2 by agriculture, forests, fossil fuel combustion, and human respiration (West *et al.*, 2011). In addition, surface fluxes over croplands were also estimated by eddy covariance (Meyers & Hollinger, 2004; Verma *et al.*, 2005) and used to evaluate bottom-up inventory methods and as observational data for crop phenology models (Lokupitiya *et al.*, 2009) used by the inversions.

Our primary objective in this study was to compare two sets of regional inversion estimates for the MCI region to a bottom-up inventory of fluxes. Estimates from a third inversion were also included, CarbonTracker (CT), which is a global scale inversion that does not use the finer scale network of observations in the MCI region. This inversion served as a standard for comparison to evaluate the influence of the higher density network on the inversion results, and we anticipated that the regional inversions would provide a more accurate estimation of CO_2 flux in the MCI study. Our secondary objectives were to explore reasons for differences between the inversion at both regional and subregional scales, with a primary focus on atmospheric transport, boundary inflow of CO_2, and *a priori* CO_2 flux estimates. This research extends work of Lauvaux *et al.* (2012a,b), incorporates CO_2 flux estimates from the operational CT system (Peters *et al.*, 2007), and presents new results for the MCI following the methodology of Schuh *et al.* (2010). The three inverse analyses presented span a range of spatial domains from global to regional, and also a range of resolutions and different techniques for regularization. Comparing their results allows us to explore, for the first time, the strengths and weaknesses of many methodological choices in regional carbon analysis for an intensive campaign (MCI) in which we have uniquely detailed independent data from the bottom-up inventory.

Materials and methods

Observational data

The two regional inversions both used data from a ring of five towers (Miles *et al.*, 2012; denoted from here on as the 'Ring'). These five sites (Fig. 1) were located in the MCI region of the NACP (Ogle *et al.*, 2006) and were outfitted with Picarro cavity ring down analyzers (Crosson, 2008). Hourly averages were computed from mixing ratios of CO_2 recorded every 2 s, with daily calibrations. The analyzers had related measurement errors that were approximately 0.2–0.3 ppm for the hourly average mixing ratio data used in the two inversions (Richardson *et al.*, 2012). The towers were instrumented beginning in May 2007. In addition to these data, both inversions used calibrated CO_2 data from the 40 m Missouri Ozarks Ameriflux tower (Stephens *et al.*, 2011) at the southern edge of the domain as well as NOAA-ESRL data from the WLEF tall tower in Wisconsin at the northern end of the domain and the WBI tall tower in the center of the domain.

Inversions

Most trace gas inversions use the same basic principles and structure that includes observations of trace gas concentrations, *a priori* estimates for trace gas fluxes, a mapping from fluxes to observations based upon an atmospheric transport model and an optimization of trace gas fluxes to minimize residuals between modeled trace gas concentrations and observed trace gas concentrations. There is a rich literature on the subject and several applications to CO_2 fluxes (Tarantola,

1987; Enting *et al.*, 1994; Evensen, 1994; Bishop *et al.*, 2001; Whitaker & Hamill, 2002; Tippett *et al.*, 2003; Zupanski, 2005; Peters *et al.*, 2007; Lokupitiya *et al.*, 2008). The goal of all three inversions in this article, labeled as the Penn State University (PSU) inversion, Colorado State University (CSU) inversion, and CT inversion, is to provide time-varying mean and covariance estimates for a set of spatial CO_2 fluxes covering the MCI region that are consistent with observed CO_2 concentrations. A simplified flowchart of the atmospheric inversion technique is provided in Fig. 2 and the main differences among the three inversion frameworks are summarized in Table 1. After describing the domain for each inversion, a summary of differences among the three frameworks is given with respect to the following components (listed in Fig. 2): 'Optimization', 'Atmospheric Transport', '*A priori* CO_2 fluxes', 'Boundary Inflow CO_2', and 'Observed CO_2'.

Spatial domain and resolution. The PSU inversion was run on a rectangular domain which overlapped portions of the non-rectangular MCI domain. Consequently, estimates for the PSU inversion were lacking for some areas in the MCI and were provided for some areas not in the MCI. As a result, we often present estimates for two areas, (i) the full MCI and (ii) the intersection of the PSU inversion domain and the MCI, which covers approximately 71% of the MCI domain. The CSU domain consisted of most of North America and extended out into the oceans to the east and west. Both domains are shown in Figure A1. The CT domain is global.

The CSU inversion domain consisted of a grid of 200 km by 200 km gridcells over most of North America with higher resolution grid of 40 km by 40 km grid cells over the MCI,
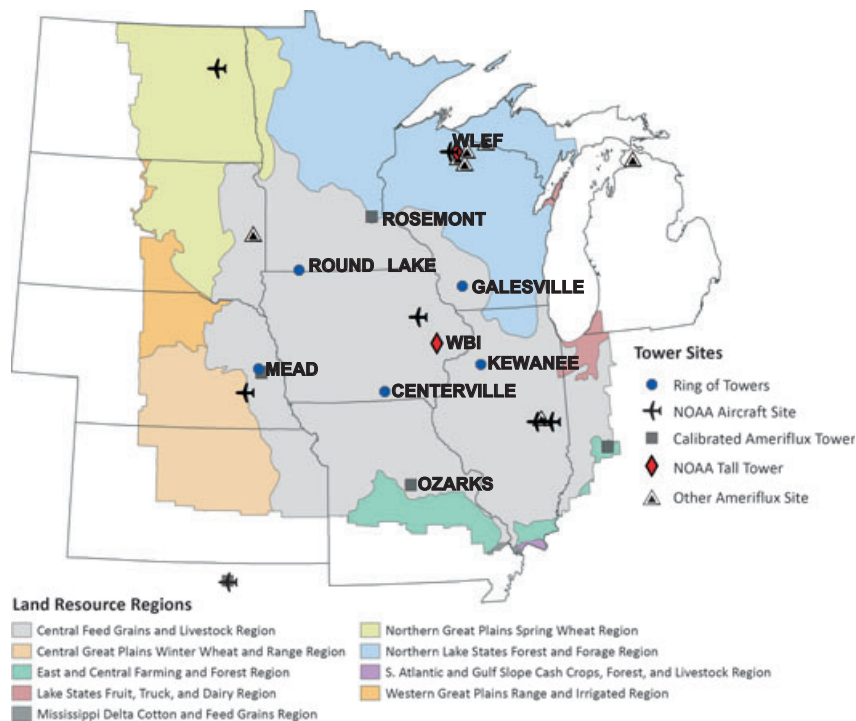

Fig. 1 Map of MCI domain located in north central United States.

covering the entire underlying transport grid. The PSU inversion domain consisted of a grid of 20 km by 20 km gridcells over their transport grid. Both can be seen in Figure A1. The CSU and PSU inversion systems are grid based and allow flux adjustments to each individual grid cell of their inversion domain, relative to constraints imposed by *a priori* flux covariances. The CT inversion grid consists of ecoregions as seen in Figure A2. The CT system scales each individual ecoregion's net ecosystem exchange (NEE) up or down each week and does not have the ability to provide any sub-ecoregion level flux adjustments (i.e. all cells are adjusted in the same manner within the region). The effect of the inversion resolution is tightly coupled to the *a priori* covariance assumptions which will be discussed later. It is important to note that due to the sparseness of available CO$_2$ observations, the resolution of the inversion domain is coarser than that of the underlying transport and *a priori* fluxes.

Optimization and temporal resolution. The CSU inversion technique is a weekly sequential Bayesian batch inversion providing optimized total respiration (OPT_TRESP) and gross primary production (OPT_GPP) on a weekly time scale at 40 km by 40 km over the MCI and 200 km continentally. *A priori* total respiration (TRESP) and gross primary production (GPP) are independently 'corrected' via regression factors, β_{TRESP} and β_{GPP} applied to the *a priori* fluxes. The model and associated cost function, $F(x)$, for a particular week, or 'cycle' are as follows:

$$OPT\_TRESP(x,y,t) = \beta_{TRESP}(x,y)TRESP(x,y,t) \quad (1)$$

$$OPT\_GPP(x,y,t) = \beta_{GPP}(x,y)GPP(x,y,t) \quad (2)$$

$$OPT\_NEE(x,y,t) = OPT\_RESP(x,y,t) - OPT\_GPP(x,y,t) \quad (3)$$

$$F(\beta) = \frac{1}{2}[(\beta - \beta_0)^T B_{\beta-\beta_0}^{-1}(\beta - \beta_0) + (H(\beta \cdot flux_{prior}) - obs)^T R^{-1}(H(\beta \cdot flux_{prior}) - obs)] \quad (4)$$

where B and R are the associated covariance matrices for the *a priori* flux corrective factor errors and the model/data mismatch, where β is the true but unknown correction factor on the fluxes and β_0 is the assumed correction factor, *a priori*. H is the observation operator providing the mapping from the flux space to concentration space and *obs* is the observed CO$_2$ vector.

The PSU inversion technique is a weekly sequential Bayesian batch inversion providing optimized estimates of daytime NEE and nighttime NEE on a 7.5 day time scale at 20 km by 20 km spatial resolution. In contrast to optimizing 'correction factors' as the CSU inversion does, the PSU inversion directly optimizes the fluxes. The associated cost function is as follows:
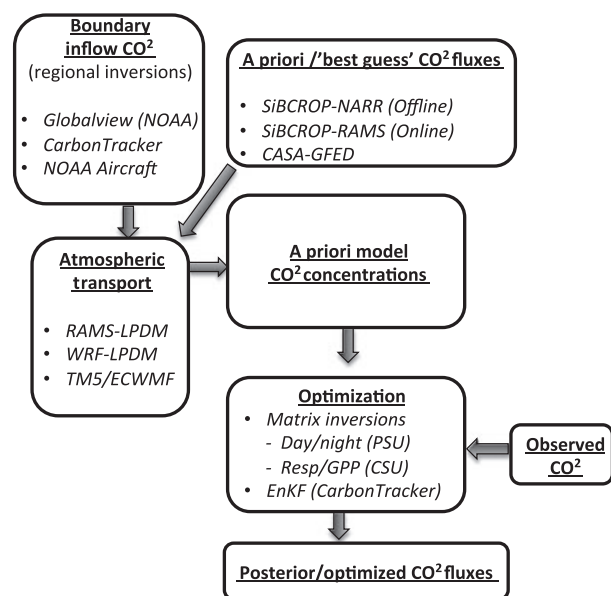

Fig. 2 Flowchart of atmospheric inversion process.

Table 1 Comparison of inversion model components

	CarbonTracker	CSU (SiB-RAMS-LPDM)	PSU (WRF-LPDM)
Inversion method	Ensemble Kalman filter	Synthesis Bayesian	Synthesis Bayesian
Transport	TM5	BRAMS 3.2*	WRF-Chem
Land surface model[†]	TESSEL	SiB3-CROP	NOAH
A priori CO$_2$ fluxes/photosynthesis model type	CASA (LUE)	SiB3-CROP (Farquhar)	SiB3-CROP (Farquhar)[‡]
Domain	Global	Continental (North America)	Regional
Transport resolution	3 × 2deg (1 × 1 deg nest)	40 km	10 km
Inversion resolution	Ecoregions (Olsen)	40 km/200 km nest[§]	20 km
Boundary CO$_2$	None (global)	CarbonTracker and GlobalView	Aircraft-corrected CarbonTracker

*BRAMS 3.2 was used as the basis for the transport model but the code has undergone numerous changes, fixes, and improvements over the last decade at Colorado State University.
[†]The LSM used to drive the meteorology in the inversion, not necessary consistent with the LSM used to generate the *a priori* CO$_2$ fluxes.
[‡]CarbonTracker posterior CO$_2$ fluxes were also used in Lauvaux *et al.* (2012a,b) but not shown here.
[§]See notes in Inversions section.

$$F = \frac{1}{2}[(\text{flux} - \text{flux}_{\text{prior}})^T B^{-1}_{\text{flux}-\text{flux}_{\text{prior}}}(\text{flux} - \text{flux}_{\text{prior}})$$
$$+ (H(\text{flux}) - \text{obs})^T R^{-1}(H(\text{flux}) - \text{obs})] \qquad (5)$$

where B and R are the associated covariance matrices for the *a priori* flux errors and the model/data mismatch. H is the observation operator providing the mapping from the flux space to concentration space and *obs* is the observed CO_2 vector. We note that the PSU inversion was run from June through December of 2007 due to its domain and dependency on the Ring data which began in June 2007. Where annual totals were required, *a priori* CO_2 distributions were used. This is not likely to be a critical limitation to the comparison, however, because the dominant fluxes are occurring between June and August. In addition, the PSU inversion uses an *a priori* annual flux consistent with the removal of harvested crops and thus one would not expect large differences in the optimization during January through May, when respiration is the primary CO_2 flux.

The NOAA 'CT system is based on a sequential ensemble Kalman filter (EnKF) framework and provides optimization of NEE from 2000 through 2009 on a weekly time scale at the resolution of 'ecoregions'. The correction to NEE is performed multiplicatively similar to the CSU inversion although the complete procedure is more complicated (Supporting Information, Appendix A2). Although the statistical procedure is applied to ecoregions, the results are often presented as the ecoregion correction factor applied to the higher resolution underlying *a priori* flux field, which gives an artificial sense of precision. We present mean results from CT in this fashion but use fractional ecoregion-wide uncertainty for the variability estimates.

Atmospheric transport. The WRF-Chem (Skamarock *et al.*, 2005) was used for transport by the PSU inversion system at a resolution of 10 km by 10km. A CSU version of the Brazilian Regional Atmospheric Modeling System (BRAMS) was used for transport in the CSU model at a resolution of 40 km by 40 km (Pielke *et al.*, 1992; Denning *et al.*, 2003; Nicholls *et al.*, 2004; Wang *et al.*, 2006; Corbin *et al.*, 2010; Schuh *et al.*, 2010). Transport fields are provided for CT by the TM5 model (Krol *et al.*, 2005), and those winds are derived from the ECMWF operational forecast model. Model resolution is 6° by 4° globally with nests down to 1° by 1° over the United States. The main difference here is that the regional models will be more accurate at resolving synoptic scale transport, i.e. storms, and vertical transport near the surface due to more highly resolved vertical grids.

The Lagrangian particle model LPDM (Uliasz & Pielke, 1991; Uliasz, 1993, 1994, 1996) is used by both PSU and CSU. It effectively acts as a transport adjoint (i.e. 'inverse') by diagnosing turbulent motions in the atmosphere as a function of high time resolution fields of zonal and meridional winds, potential temperature, and turbulent kinetic energy output from a parent mesoscale model. This allows for the creation of a Jacobian matrix representing the partial derivatives of CO_2 concentration (at a fixed location) with respect to the surrounding fluxes of CO_2. The details of the Lagrangian model that produces the particle movements from the parent mesoscale model can be found in Uliasz (1994) and there are many applications in the literature (Zupanski *et al.*, 2007; Lauvaux *et al.*, 2008, 2012b; Schuh *et al.*, 2009, 2010). Further details on this technique can be seen in the Supporting Information, Appendix D1.

A priori CO_2 fluxes. The inversions use *a priori* CO_2 flux distributions that are Gaussian in nature and are thus composed of mean and covariance information.

Means: The *a priori* flux assumptions for the CSU and PSU regional models are based on the Simple Biosphere model (SiB), a land surface parameterization scheme originally used to compute biophysical exchanges in climate models (Sellers *et al.*, 1986), but later adapted to include ecosystem metabolism (Denning *et al.*, 1996; Sellers *et al.*, 1996). The photosynthesis in SiB follows the Farquhar approach (Farquhar *et al.*, 1980). A phenology-based crop module was then added to SiB and is detailed in Lokupitiya *et al.* (2009). This model was used in two ways. First, hourly CO_2 fluxes were calculated from offline runs of the model driven by North American Regional Reanalysis meteorological data, at 40 km by 40 km resolution and 10 km by 10 km resolution, respectively, with three sub-gridscale landcover patches for each configuration. Secondly, the CSU model also ran test cases in which the SiB-CROP model was run in coupled-mode inside of BRAMS in an effort to provide consistency between the modeled CO_2 fluxes and the meteorological data.

For CT, the *a priori* NEE estimates are recreated from CASA-GFEDv2 model runs of the Carnegie-Ames Stanford Approach (CASA) biogeochemical model, which employs a light use efficiency (LUE) photosynthesis model based upon AVHRR NDVI and year-specific weather. Global 0.5° by 0.5° resolution monthly output from the CASA-GFEDv2 model (van der Werf *et al.*, 2006) for GPP and TRESP is scaled down to 3 hourly fluxes using a simple Q_{10} relationship and a linear scaling for photosynthesis based upon ECMWF analyzed meteorology. These are then differenced to provide diurnally varying NEE, while conserving monthly mean NEE in a manner similar to that of Olsen & Randerson (2004). The most significant differences between the CT inversion and regional inversions is the lack of an explicit crop model and the lack of explicit sub-daily predictions of C exchange in CASA-GFEDv2.

Covariances: For the CSU inversion, *a priori* covariance matrices for the multiplicative biases on GPP and TRESP (β factor in Eqn 4) were formed by constructing isotropic exponential spatial covariance structures over North America with decorrelation length scales of 500 and 1000 km (more information available in the Supporting Information, Appendix A4) and scaling them to 0.2, which amounts to standard deviations of 20% on GPP and TRESP. *A priori* covariance assumptions for the PSU inversion, i.e. $B_{\text{flux}-\text{flux}_{\text{prior}}}$ (see Eqn 5), included smaller decorrelation length scales (exponential covariance) of approximately 300 km, compared to the CSU inversion which generally employed 500 and 1000 km for results shown in this article. The smaller decorrelation length scales of the PSU inversion were further decreased by modeling the covariance length scale as a function of ecosystem type, resulting in

equivalent isotropic decorrelation length scales of approximately 100 km. The temporal correlations were calculated consistent with Lauvaux et al. (2009). More information on a priori covariance of flux fields in the PSU inversion is available in the Supporting Information, Appendix A4 and Lauvaux et al. (2012b). There are no explicit spatial correlation assumptions in CT due to the use of larger ecoregions in its optimization but the a priori standard deviations are 0.85 on each ecoregion, amounting to a standard deviation of 85% of a priori NEE.

The main difference in covariance structures between the inversions is directly related to the ability of the inversions to assign, or adjust the prior based on the observed CO$_2$ concentrations, on a finer scale within the MCI region. The PSU inversion has the most freedom to make fine scale adjustments due to smaller spatial correlations followed by the CSU inversion with a moderate ability to correct subregional fluxes. The CT inversion is limited to multiplicative corrections on NEE which are equally applied across the ecoregions (Figure A2) and thus is the most restricted.

Boundary inflow CO$_2$. While global inversion systems like CT inherently have no boundaries, regional inversion results can be very sensitive to boundary conditions, i.e. the inflow of CO$_2$ from the boundaries of the model domain (Goeckede et al., 2010b; Gourdji et al., 2012). The CSU inversion benefits from much lower variability in boundary inflow due to its eastern and western boundaries being over the ocean. This will make boundary bias corrections easier than correcting for boundary inflow over locations with more variability in CO$_2$ fluxes occurring in the middle of the continent (PSU).

However, the distance between the boundaries of the domain and the boundaries of the MCI make the CSU inversion dependent upon optimized fluxes over the continent with much weaker observational constraints. In particular, the CSU inversion utilizes inflow estimates (optimized CO$_2$) from the global CT inversion system with a bias correction based on interpolated global CO$_2$ from NOAAs GlobalView (GV) product while the PSU inversion also utilizes optimized CT CO$_2$ bias corrected with routine NOAA aircraft flights near their domain boundaries (Lauvaux et al., 2012b). We provide results with both bias-corrected and uncorrected CT inflow for the CSU inversion and detail the bias correction procedure in the Supporting Information, Appendix A3.

Observed CO$_2$. The PSU and CSU inversions both used the Ring data while using slightly different data streams from NOAA tall towers at WLEF in Wisconsin and WBI in Iowa. The PSU inversion used data from 122 m at WLEF and 99 m at WBI meters to be consistent with the other tower heights while the CSU inversion used the highest levels for WLEF and WBI which are 396 and 379 m, respectively. The full observational constraints for the PSU and CSU inversions are summarized in Table 2. As mentioned earlier, the PSU inversion only ran from June through December. The CSU and CT inversions used data from the NOAA WLEF and WBI tall towers from January to May and otherwise were constrained by the sparser continental network. The effect of the data gap on the PSU inversion is probably minimal in this study because of the a

priori knowledge that a large percentage of the Net Primary Production is removed from the study region and not available for decomposition, however, we emphasize that, in general, this should not be the case.

The CT inversion is nearly real-time operational and uses global *in situ* as well as flask-collected data in its flux optimization (Peters et al., 2007). An important note is that it does not use the Ring data situated in the heart of the MCI region (Miles et al., 2012). Modified runs were performed with the data from the Ring for 2008. However, the inclusion of the data did not significantly alter the cropland flux estimates, instead increasing uptake in upwind grassland/shrub areas to the west and no additional diagnosis was performed to determine the exact cause of the insensitivity of local fluxes to the Ring data. Therefore, the original and publicly available flux estimates (CarbonTracker, 2009) were used in this study. The lack of any sensitivity of CT to the Ring data, and inability to optimize subregional fluxes, were two particular reasons that mesoscale inversions were employed in this study.

Specified model-data mismatch errors (the R matrix in Eqns 4 and 5) correspond to *posterior* model fits of the observations and thus, theoretically, are generally not available before the inversion step is run. The errors in the CSU inversion are thus formed by running the inversion initially using differences between the a priori modeled CO$_2$ concentrations and the observations and then reducing this a priori error by a somewhat arbitrary 40%. To create the model-data mismatch in the PSU inversion, R, the framework used a combination of projections of boundary layer depth errors and forward-adjoint consistency to create the errors. The CT system uses subjective choices for the errors which depend upon the location of the observing tower and how well the authors felt that the transport model, TM5, could reproduce local atmospheric motions there (see Supplementary Material, Peters et al., 2007). All three inversions calculate the chi-square innovation statistic and use this value to scale the a priori model-data mismatch to guarantee that they do not overestimate or underestimate the model-data mismatch a priori, which reduces some of the apparent dependency on the initial setting of R described above.

Inventory methods

A bottom-up CO$_2$ flux inventory was compiled for the MCI region for evaluating against the atmospheric inversion results. This inventory utilizes data on forest biomass, harvested woody products, and agricultural soil C from the US Greenhouse Gas Inventory (EPA, 2010; Ogle et al., 2010), in addition to fine resolution data on fossil and biofuel CO$_2$ emissions (Gurney et al., 2009), CO$_2$ uptake by agricultural crops and grain harvest (West et al., 2011), and CO$_2$ losses through livestock and human respiration associated with agricultural products (West et al., 2011). Uncertainties were derived from a Monte Carlo analysis in which probability distribution functions were developed for the flux estimates from each of the sources and random draws were made to produce 100 realizations of the total flux in the region. The carbon inventory was constructed on an annual time frame, due to temporal limitations in the FIA and harvest statistics, and was derived from

Table 2 CO$_2$ observations

Site	Height	Contact	PSU inversion	CSU inversion	CarbonTracker inversion
Argyle, ME	107 m	A. Andrews, NOAA-ESRL	Outside domain	12:00–18:00 LST	12:00–16:00 LST
Centerville, IA	110 m	N. Miles/S. Richardson, Penn State U	All hours	12:00–18:00 LST	Not used
Candle Lake, BC	30 m	D. Worthy, EnviroCanada	Outside domain	12:00–18:00 LST	12:00–16:00 LST
Fraserdale, ON	40 m	D. Worthy, EnviroCanada	Outside domain	12:00–18:00 LST	12:00–16:00 LST
Galesville, WI	122 m	N. Miles/S. Richardson, Penn State U	All hours	12:00–18:00 LST	Not used
Kewanee, IL	140 m	N. Miles/S. Richardson, Penn State U	All hours	12:00–18:00 LST	Not used
Park Falls, WI	122 m/396 m	A. Andrews, NOAA-ESRL	All hours (122 m)	12:00–18:00 LST (396 m)	12:00–16:00 LST (396 m)
Lac Labiche, AB	10 m	D. Worthy, EnviroCanada	Outside domain	12:00–18:00 LST	12:00–16:00 LST
Metolius, OR	33 m	M. Goeckede/Beverly Law, Oregon State University	Outside domain	12:00–18:00 LST	Not used
Mead, NE	122 m	N. Miles/S. Richardson, Penn State U	All hours	12:00–18:00 LST	Not used
Missouri Ozarks, MO	30 m	N. Miles/S. Richardson, Penn State U	All hours	12:00–18:00 LST	Not used
Round Lake, MN	110 m	N. Miles/S. Richardson, Penn State U.	All hours	12:00–18:00 LST	Not used
Sable Island, NS	25 m	D. Worthy, EnviroCanada	Outside domain	12:00–18:00 LST	12:00–16:00 LST
West Branch, IA	99 m/379 m	A. Andrews, NOAA-ESRL	All hours (99 m)	12:00–18:00 LST (379 m)	12:00–16:00 LST (379 m)
Moody, TX	457 m	A. Andrews, NOAA-ESRL	Outside domain	12:00–18:00 LST	12:00–16:00 LST

Observations used by inversions. All towers used by PSU inversion were used by CSU inversion. Additional towers were used by CSU due to larger domain size. CarbonTracker use of data, common to PSU and CSU inversions, is shown as ancillary information. CarbonTracker is a global inversion framework and thus makes use of large amounts of data outside of North America which are not detailed here. Although custom filtering of observations is inversion dependent as well as dependent upon quality flags/operatibility of the towers, the times for considered data in each inversion are given in the table. PSU inversion uses all hours but with different weightings for different times of day and therefore nocturnally collected data is usually weighted more weakly, see Lauvaux *et al.* (2012b).

spatial data with a US county level resolution. For example, US counties in Iowa are very homogenous in size and shape and have a resolution of approximately 40 km by 40 km and thus the county sizes are comparable to the 0.5° by 0.5° resolution grid cells used to display the inventory.

Results

Bottom-up annual inventory of CO$_2$ fluxes

Based on the bottom-up inventory analysis, sources of CO$_2$ in the MCI domain are dominated by fossil fuel combustion (262 TgC source), in particular the city of Chicago (Gurney *et al.*, 2009). Inversions usually consider fossil fuel fluxes as 'known' and without error and optimize the nonfossil fuel CO$_2$ fluxes due to better knowledge of fossil fuel combustion when compared to natural biospheric fluxes and difficulties optimizing very localized point sources of CO$_2$. The nonfossil fuel inventory data show a net CO$_2$ uptake of 135 TgC for 2007 and are shown in Fig. 3. The flux is dominated by

the harvest and export of grain from the region (West *et al.*, 2011). Smaller sources and sinks associated with feedlots, forests, other natural vegetation, and human respiration also contribute to the total. Uncertainty for the nonfossil inventory is largely dominated by the harvest product while relative uncertainties, i.e. standard deviation in NEE as function of mean NEE, is largest for the FIA forest product. The spatial correlations in the inventory impact the region-wide uncertainty and can be better understood by an investigation of Fig. 3 of Cooley *et al.* (2012). Using a Monte Carlo analysis based on uncertainties in each component flux, we constructed 95% confidence limits on the CO$_2$-C balance (net fossil fuels) of the MCI domain which resulted in a sink of −104 to −204 TgC for 2007 (mean: −135 TgC).

Annual CO$_2$ fluxes from inversions

The results for all three inversions are statistically indistinguishable from the inventory results for the annual

Inventory 2007 annual NEE mean (GgC per 0.5°x 0.5°)   Inventory 2007 annual NEE S.D. (GgC per 0.5°x 0.5°)
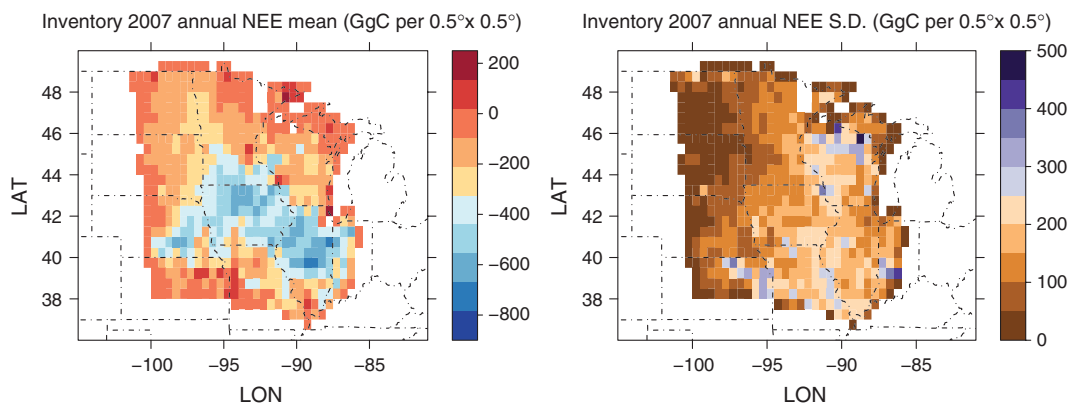
Fig. 3 Annual NEE estimate by the inventory components. Mean estimates are shown in left panel and standard deviations are shown on right side. Note that the distribution of the inventory is not necessarily Gaussian and therefore, in a rigorous sense, the standard deviation is simply a measure of uncertainty.

net CO_2 budget of the region (Fig. 4). After correcting the regional inversions for boundary inflow, all three inversion estimates show a slightly stronger sink than the inventory (CT = -155 ± 173 TgC, PSU = -140 ± 26 TgC for reduced 'PSU domain', CSU = -145 ± 29 TgC). The difference in the inversion system results was primarily influenced by the *a priori* flux uncertainty estimates, i.e. the initial range for the 'best guess' NEE. The CSU inversion used independent $\pm 20\%$ standard deviations for GPP and TRESP fluxes which is equivalent to an enormous range of possible flux results. The particular choice of 20% comes from the desire to keep correction factors positive, ensuring positive optimized GPP and TRESP. These conservative choices introduce flux scenarios that could be well outside the range of reasonableness, for example a 20% increase in annual TRESP and 20% reduction in annual GPP, relative to a balanced biosphere would cause a C source on the order of 300 TgC. It is important to note that the variability around the CT estimate is unrealistically large. This is well known and documented (CarbonTracker, 2011). However, the predictions generally appear more accurate than would be inferred from the formal flux uncertainty.

The three inversions produce similar spatial patterns in annual NEE compared to the inventory, with an important sink in the center of the domain corresponding roughly to the highest density of agricultural area (Fig. 5). However, at finer scales, the location of the maximum of uptake and the shape of the sink area varies substantially among the inversions. To evaluate this pattern, the inversion results were compared to the inventory data from the individual grid cells. Scatterplots of annual NEE values for the inversions vs. the inventory are shown in Fig. 6. Correlations with the inventory are higher for the CSU ($r = 0.76$) and PSU ($r = 0.55$) inversion results. The weaker correlation of

the CT results with the inventory ($r = 0.36$) can be seen along with a bimodal feature in the figure.

Much of the spatial structure in the estimated maps of net annual flux is driven by the structure of the Bayesian *a priori* mean and the optimization method in each inversion model, i.e. the degree to which the inversion framework allows for independent adjustments to the *a priori* fluxes given the observed CO_2 data. The CSU inversion shows a strong correlation with the *a priori* June/July/August uptake in the region, but with a weaker C sink in Illinois and a stronger C sink in western Iowa. The spatial resemblance to the inventory is likely due to the strong 500–1000 km *a priori* decorrelation lengths used in the inversion and the strong summer time CO_2 deficit. Using a 500-km decorrelation length as an example, and noting that the width of Iowa is about 500 km, the inversion would assume that a weekly multiplicative error in GPP on one end of Iowa is correlated with an error in GPP on the other end of Iowa at a level of 0.37, *a priori*. Posterior correlations were reduced by about half although the reduction was different for GPP and TRESP and not isotropic, instead following the sampling gradient. There were no significant differences between using 500 and 1000 km on the regional NEE (Table 3).

The smaller *a priori* decorrelation length scales used in the PSU inversion, approximately five times less that those used in the CSU inversion, lead to much finer spatial adjustments in the *a priori* fluxes within the region. The PSU inversion shows a very large sink in the eastern part of the domain (northern Illinois), 20–30% larger than the inventory estimate in the area, as well as a stronger more diffuse sink to the northeast of the domain, an area of larger uncertainty in the inventory.

In contrast, the strongest sink for the CT inversion is located in the extreme northwest portion of the MCI
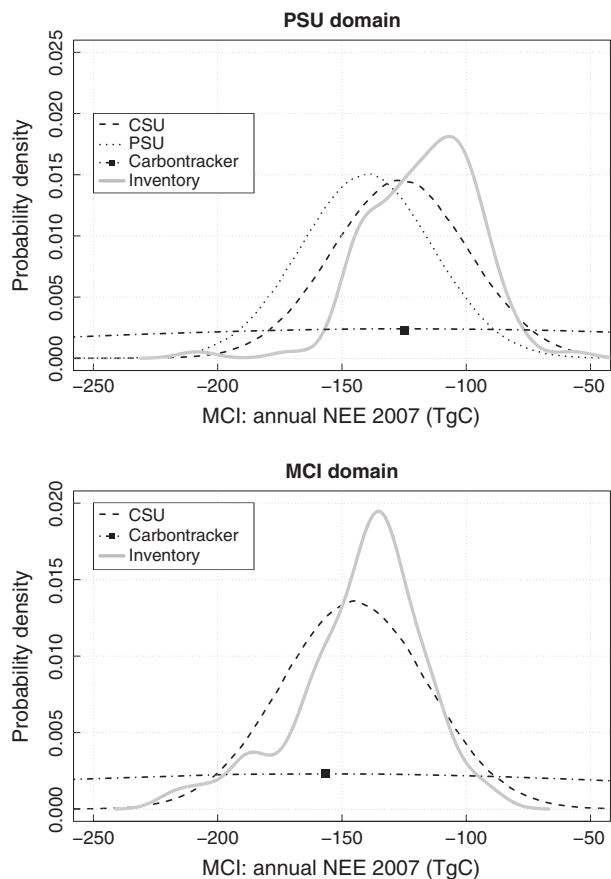
Fig. 4 Densities for annual NEE for inversion results and inventory (2007). Top panel shows results for the intersection of the PSU inversion model domain and MCI domain while bottom panel shows results for the entire MCI region. PSU inversion is based on SiB3-CROP offline prior. CSU inversion is also based on SiB3-CROP offline prior with GV-bias-corrected CT inflow. These results include explicit variability estimates that were constructed for the inventory using a Monte Carlo anlysis and variability estimates that arise naturally from the matrix-based atmospheric inversion procedure. CarbonTracker variability was approximated by summing fractional ecoregion-wide variability for each ecoregion which occurred in the MCI. Variability estimates were unrealistically large and thus no effort was made to include the whole pdf in the image. The CT mean is indicated by a filled square. The variability induced by varying inflow CO_2 or underlying transport model characteristics is not implicitly included here but can be seen in Table 3.

although the overall sink appears more diffuse. This is likely due to a strong flux in the prior for this particular area of the MCI and may be a result of inadequate crop modeling in CASA, which does not explicitly account for agricultural crops. Northern portions of the MCI have strong influences from soybeans and spring wheat, but these crops do not assimilate as much carbon during the peak of summer according to the inventory and eddy covariance studies (Lokupitiya *et al.*,

2009), suggesting that a mix of wheat and soybeans contributes a weaker NEE signal than a mix of soybeans and corn. Overestimating the flux in the northwest portion of the MCI led to the bimodal distribution in flux mismatch between the CT inversion and inventory that was apparent in Fig. 6.

Although not included in Fig. 4, we also assessed the variability in CO_2 inflow and its effect on the PSU and CSU inversions. For the CSU inversion, this sensitivity can be viewed in Table 3 while a general discussion of the inflow uncertainty for both regional inversions is provided later.

Transport and boundary inflow considerations

The transport and inflow boundary conditions could also influence the pattern and strength of fluxes within the region. However, the transport fields produced from the mesoscale models displayed a surprising amount of similarity. Despite different mesoscale models, PBL schemes, land surface models, and external forcing scales in time and space, differences in time-space integrated afternoon observation footprints for the towers in the aaa'ring' remained on the order of 20% of the absolute signal or less, varying as a function of distance from the tower (Supporting Information, Appendix D). Among the differences between the transport fields that could not be immediately explained, was the sensitivity to surface fluxes as a function of distance from tower. The RAMS model (CSU) appeared to show weaker sensitivity in the local vicinity of the tower and a stronger long-distance sensitivity than the corresponding WRF model (PSU).

In addition, regional inversion results can be sensitive to boundary conditions, i.e. the inflow of CO_2 at the boundaries (Goeckede *et al.*, 2010b; Gourdji *et al.*, 2012). We evaluated the influence of inflow boundary conditions on the CSU inversion by using the CT-optimized CO_2 as inflow with and without corrections for a known Northern Hemispheric seasonal bias. Bias correction to the CT optimized CO_2 inflow reduced the CSU sink in the MCI by approximately 33%, from 174 TgC to 117 TgC in the 'online' case, while reducing the continental sink (data not shown) by 62% (1.6–0.6 PgC) providing better agreement with independent CO_2 inventory estimates for North America (King *et al.*, 2007). This inflow sensitivity is consistent with the findings of others who used similar methodologies (Gourdji *et al.*, 2012). Furthermore, this adjustment to boundary inflow in the CSU inversion appeared, to first order, to simply shift the posterior annual NEE up or down. Similar results are summarized for the PSU inversion in the Supporting Information (Appendix A3) and Lauvaux *et al.* (2012b).
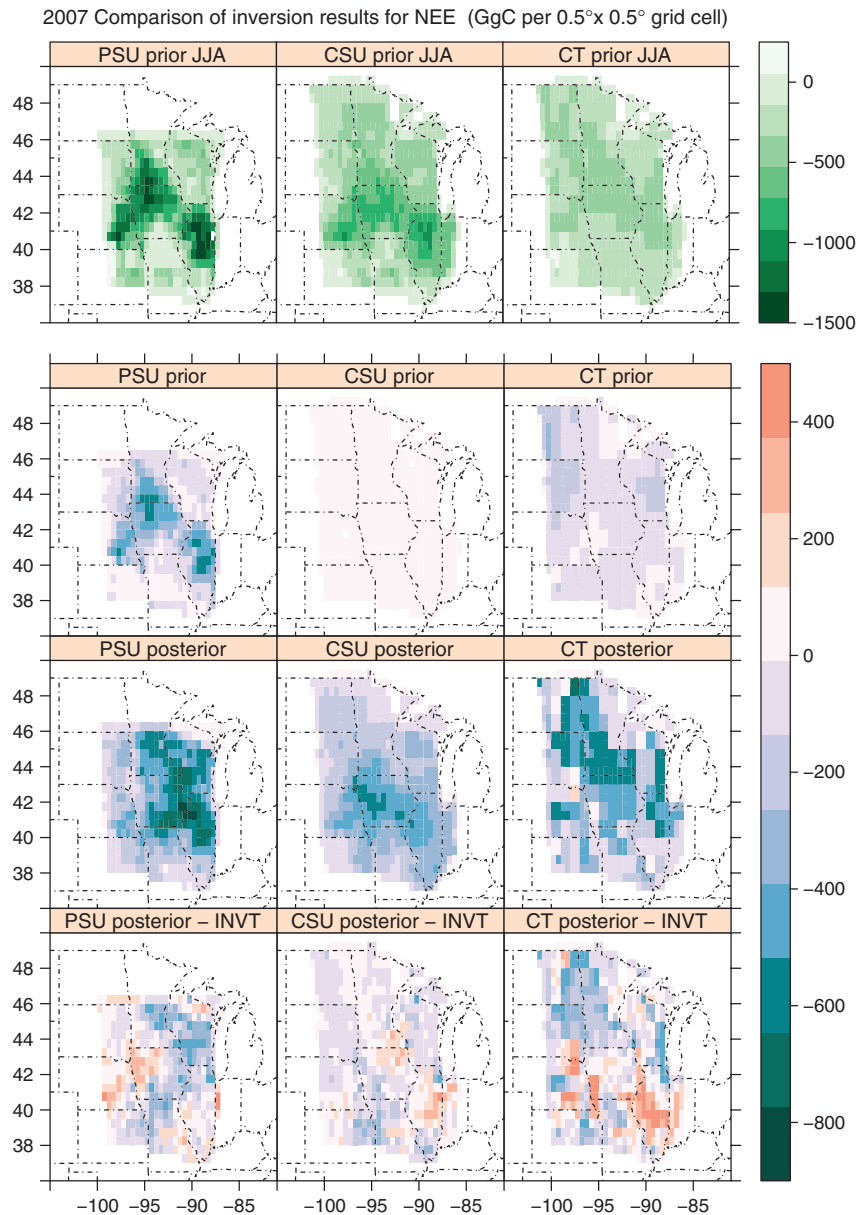
Fig. 5 Each panel name is composed of the following(i) inversion model, (ii) 2007 for annual total or JJA2007 for June/July/August sum, and (iii) 'pr' for *a priori* and 'post' for posterior flux. *A priori* annual 2007 NEE estimates are shown in middle row with posterior annual 2007 NEE estimates shown in the bottom row. The bottom row consists of differences between the inversion models and the inventory (INVT). PSU inversion is based on SiB3-CROP offline prior with residual 109 TgC harvest sink. CSU inversion is also based on same prior (and underlying seasonality), but with residual harvest sink balanced by respiration annually to induce net zero NEE and uses GlobalView bias-corrected CT inflow. The top row shows the June/July/August total NEE for each prior flux which is indicative of the spatial signal of strong summer crop carbon drawdown. A few grid cell values were truncated at the bounds of the color bar for visualization purposes. Multiplying fluxes by 0.45 gives approximate conversion into grams per square meter.

We conducted an additional test by evaluating the CSU inversion results outside of the MCI for consistency with the bias-corrected inflow used by the PSU inversion. Inflow estimates for the Kewanee tower were calculated from the CSU inversion by subtracting out the effect of the PSU inversion region from the CSU modeled Kewanee CO₂. In this fashion, we were able to compare the expected inflow at the Kewanee tower from the boundaries of the PSU inversion region, for both the CSU and PSU inversion systems. Posterior inflow estimates for the CSU inversion at the boundary had a correlation of 0.82 compared to 0.41 for the *a*
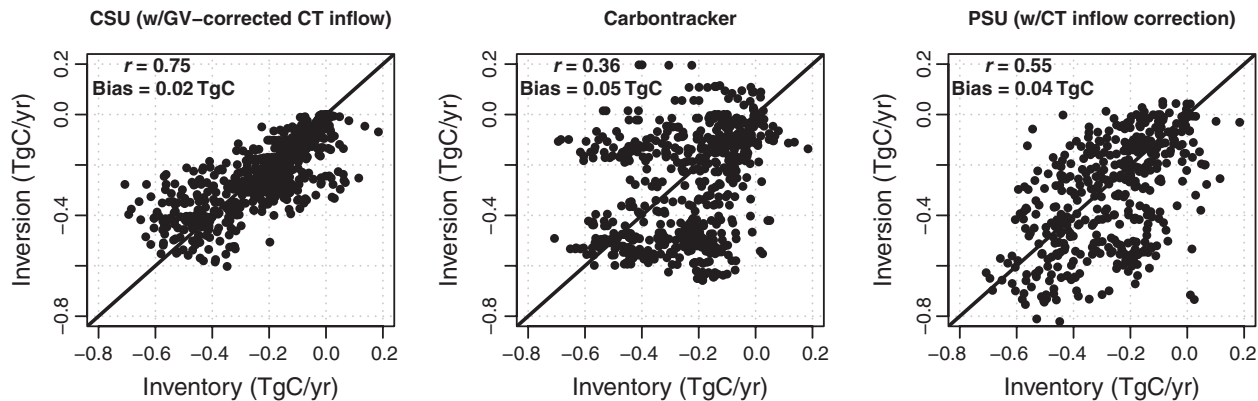
Fig. 6 Plots of inventory estimates vs. inversion for annual 2007 NEE. Each pixel of Fig. 4 is represented as a datum in the figure. PSU inversion is based on SiB3-CROP offline prior. CSU inversion is also based on SiB3-CROP offline prior with GV-bias-corrected CT inflow.

priori inflow estimates and the mean difference between the CSU inflow estimate and the PSU bias-corrected inflow estimate dropped from 2.8 to 1.8 ppm. Thus, despite limited towers outside of the MCI, the CSU inversion appeared to provide inflow estimates at the MCI boundary which were more consistent with the bias-corrected CT inflow. However, a positive annual difference exists in the inflows, 1.8 ppm. If this difference is allocated to the PBL, roughly 1/7 of the atmospheric column, and spread evenly over the MCI region, it appears to provide an explanation for the fact that the CSU CO_2 sinks are often 10–15% stronger than the PSU CO_2 sinks (Table 3).

Discussion

Continental and meso-scale inversions were developed for 2007 using a relatively high density of observations in the MCI region. These data were compared to a bottom-up inventory and a global inversion framework, CT, which did not assimilate the higher density of CO_2 observations in the region. NEE flux estimates are similar among inversions, even from the CT system, and are reasonable for 2007 in the sense that they are statistically consistent with the inventory. These results are promising because they show that CO_2 inversion methods can be robust, in the sense that they deliver similar inverse flux solutions which are consistent with C inventory results, despite being constructed across very different frameworks, e.g. global to continental to regional, with very different assumptions. Nevertheless, comparisons to the inventory at spatial scales finer than 100–200 km and finer temporal scales on the order of weeks (data not shown), demonstrate the value of higher resolution inversion systems that can benefit from finer scale observations in terms of recovering finer CO_2 flux patterns within a region.

The agreement of large-scale posterior CT CO_2 fluxes to the inventory, despite major differences in fine scale flux signals may be fortuitous. The minimum scale of the gradients of CO_2 resolved by the CT transport model TM5 at 1° by 1° resolution is likely in the 200–300 km range. However, the region was chosen to avoid complex meteorology induced by land-sea contrasts or complicated topography. Hence, if the observations used by CT constrain the MCI domain reasonably well, it is certainly reasonable to recover large-scale agreement in flux estimates. Nevertheless, the very nature of the coarse inversion region used by CT (Supporting Information, Appendix A1) prohibits the CT system from recovering fluxes on most scales less than the MCI region and forces strong coherence to *a priori* CASA flux patterns at higher resolutions. Furthermore, the lack of higher resolution attribution of flux errors might limit this type of inversion from being used to further future prognostic carbon cycle modeling efforts.

The PSU inversion framework uses the most highly constrained area, i.e. an area slightly larger than the Ring of towers. The advantages of this are that they use a wealth of eddy covariance tower data to help constrain the *a priori* fluxes as well as provide more flexibility spatially to adjust fluxes. This was shown in Lauvaux *et al.* (2012b) to allow some degree of robustness of the posterior flux result to distinct underlying *a priori* flux fields. Therefore, given dense enough observational coverage of CO_2, one would expect to be able to proceed toward improvements in prognostic carbon cycle modeling where this is not possible with the CT inversion system. The disadvantage of this particular inversion is that the corrections to inflow on the sides of the domain will likely be larger and more variable than those made over marine boundary layer conditions and require the use of aircraft to obtain vertical profiles.

Table 3 MCI source/sink results (due to model variations)

Inversion method	Inflow	Prior description	Prior NEE (MCI)	Post NEE (MCI)	Prior NEE (PSU Dom.)	Post NEE (PSU Dom.)	Prior NEE (PSU Dom.) (June–December)	Post NEE (PSU Dom.) (June–December)
CarbonTracker	N/A	CASA-GFED	−40 TgC	−155 TgC	−30 TgC	−125 TgC	−124 TgC	−196 TgC
PSU	Aircraft-corrected CT	SiB3-offline	N/A	N/A	−65 TgC	−140 TgC	−109 TgC	−185 TgC
PSU	Aircraft-corrected CT	CarbonTracker optimized	N/A	N/A	−154 TgC	−127 TgC		
CSU	CarbonTracker opt.	SiB3-offline	−82 TgC	−235 TgC	−75 TgC	−200 TgC	−126 TgC	−251 TgC
CSU	GV-corrected CT opt.	SiB3-offline (forced annual balance)	0 TgC	−145 TgC	−75 TgC	−127 TgC	−66 TgC	−203 TgC
CSU	GV-corrected CT opt.	SiB3-offline (dec length: 1000 km)	−82 TgC	−162 TgC	−75 TgC	−144 TgC	−127 TgC	−213 TgC
CSU	GV-corrected CT opt.	SiB3-offline (dec length: 500 km)	−82 TgC	−160 TgC	−75 TgC	−143 TgC	−127 TgC	−213 TgC
CSU	CarbonTracker opt.	SiB3-RAMS coupled	0 TgC	−174 TgC	0 TgC	−154 TgC	−62 TgC	−208 TgC
CSU	GV-corrected CT opt.	SiB3-RAMS coupled	0 TgC	−117 TgC	0 TgC	−107 TgC	−62 TgC	−177 TgC
Inventory				−135 TgC		−117 TgC		

Negative NEE indicates carbon moving from atmosphere to the biosphere. These SiB3-offline fluxes were driven from offline run of the model driven by NARR data, which were used as the driving external forcing necessary for both WRF and RAMS. Inversion results for PSU inversion are put on a full annual 2007 basis by adding *a priori* fluxes from SiB3-CROP for January–May 2007 (before MCI towers were instrumented) to both *a priori* and a posterior flux estimates for June 2007 through December 2007. PSU inversion results for the 'optimized CarbonTracker flux' case are on the native PSU grid which is slightly larger than the 'PSU grid' which is used throughout this article which represents the intersection of the native PSU grid and the MCI domain. *A priori* fluxes from SiB3-offline are characterized by a 'realistic' annual harvest sink while the 'forced annual balance' case forces NEE to zero over all gridcells by balancing total respiration with gross primary production. Typically, the *a priori* fluxes and transport are derived in a decoupled environment. However, the 'SiB3-RAMS' *a priori* fluxes are those produced as a result of the parent SiB3-RAMS simulation, which produced the transport used in the CSU inversion, i.e. coupled. 'Dec length' indicates the *a priori* decorrelation length scale, or e-folding length, used for the exponential spatial correlation in the *a priori* fluxes. This value is generally less than 300 km for PSU inversions and 1000 km for CSU, unless otherwise noted.

The CSU inversion is largely a compromise between the CT and PSU systems. Boundary inflow corrections are still necessary because of the regional nature of the inversion but are made over marine boundary sites that are generally less variable in time and space and observed with the operational NOAA flask network. This tends to preserve the *a priori* flux gradients around the perimeter of the MCI because rapid flux adjustments are not needed to force agreement between tower observations and model observations close to the model domain boundary. The disadvantage is the need for a unified framework to simultaneously model the more densely observed MCI region and the rest of the continent. This topic was studied recently (Wu *et al.*, 2011), but the heterogenous nature of the evolving CO_2 observing network probably demands continued investigation especially as satellite observations of CO_2 become available. Furthermore, the impact of estimating (i) NEE, (ii) day/night NEE, or (iii) total respiration and GPP upon the inversions is still uncertain and remains an active research question.

With respect to our secondary objectives, differences between the inversions and inventory were influenced by boundary inflow estimates of CO_2, *a priori* flux signals and differences in transport. As can be clearly seen from Table 3, the domain wide flux is most strongly influenced by the inflow estimates. Finer spatial scale flux variations then result from differences in transport and *a priori* flux patterns. Increased observations in the inversion domain should lessen the impact of the *a priori* flux assumptions, but the inflow estimate errors generally remain a systematic error, which must be corrected in an independent manner. Inflow corrections were performed using the GV NOAA product and the NOAA weekly aircraft samples as the basis of the bias correction scheme to the optimized global CT CO_2 product and significantly improved the accuracy of the inversion results we showed. This demonstrates the importance of maintaining well calibrated global CO_2 networks and in particular aircraft profile programs with respect to estimating regional carbon budgets with CO_2 data. Differences in the bias-corrected inflow estimates between the two regional inversion appeared to be the primary cause of the differences in the annual CO_2 flux estimates from the MCI region as a whole.

Posterior variance estimates of CO_2 exchange continue to be one of the most difficult estimates to make for inversion modelers. Variance estimates from these CO_2 inversion systems are sensitive to both inversion method and *a priori* covariance specifications. For example, posterior covariance from EnKF methods such as used for CT are strongly dependent upon the particular EnKF algorithm (Tippett *et al.*, 2003). The *a priori* flux variances are generally very conservative on annual scales. Standard deviations of 85% on ecoregion-wide NEE for CT and standard deviations (independent) of 20% for TRESP and GPP for the CSU inversion led to a large range of possible net fluxes; far stronger annual sources and sinks than could be possible given global constraints and thus sufficiently conservative. Shortages of ancillary information on NEE, such as spatially dense eddy covariance observations or temporally and spatially rich biomass accumulation statistics often necessitate 'broad' *a priori* covariance structures be used in inversion systems attempting to estimate fluxes over continental or larger regions. While inversion modelers can attempt to control for portions of this uncertainty, i.e. model methodology, other portions such as ancillary data to constrain the fluxes *a priori* are generally outside of their control. Nevertheless, results from this study showed that quite good agreement can result from two inversions (CSU and PSU) where different *a priori* flux uncertainties, as well as system and method, were used.

In summary, regional flux estimates from each of the three frameworks agreed well with the estimates provided by the inventory data, but the continental and meso-scale inversions were better able to recover the spatial pattern of fluxes in the region. We consider this a first step toward ascertaining feasibility of the CO_2 inversion method to produce regional carbon flux estimates as would be done under a monitoring program. Moreover, this study shows that atmospheric inversions are capable of capturing regional CO_2 flux estimates at sub-national scales, scales which will be useful for future carbon-cycle research and regional greenhouse gas initiatives. The most critical next steps are to further refine the inversion frameworks to better quantify boundary inflow uncertainty, sensitivity to a prior flux estimates, and to provide explicit characterizations of transport variability as well as leverage the most recent and comprehensive sources of data on CO_2.

Author Contributions and Acknowledgements

References

Baker DF, Doney SC, Schimel DS (2006) Variational data assimilation for atmospheric CO$_2$. *Tellus*, **58B**, 359–365.

Baldocchi D, Reichstein M, Papale D, Koteen L, Vargas R, Agarwal D, Cook R (2012) The role of trace gas networks in the biogeosciences. *EOS Transactions, American Geophysical Union*, **93**, 217–224.

Bishop CH, Etherton BJ, Majumjar S (2001) Adaptive sampling with the ensemble transform kalman filter: part 1: theoretical aspects. *Monthly Weather Review*, **129**, 420–436.

Bolin B, Erickson E (1959) *Changes in the Carbon Dioxide Content of the Atmosphere and Sea due to Fossil Fuel Combustion*. The Rockefeller Int. Press, New York.

Bolin B, Keeling CD (1963) Large-scale atmospheric mixing as deduced from the seasonal and meridional variations of carbon dioxide. *Journal of Geophysical Research*, **68**, 3899–3920.

CarbonTracker (2009) Ct-2009 CO$_2$ flux estimates. Available at: http://www.esrl.noaa.gov/gmd/ccgg/carbontracker/CT2009/ (accessed 6 January 2011).

CarbonTracker (2011) Carbontracker system documentation. Available at: http://www.esrl.noaa.gov/gmd/ccgg/carbontracker/documentation CT2011.pdf (accessed 10 January 2012).

Chen J, Davis KJ, Meyers TP (2008) Ecosystem-atmosphere carbon and water cycling in the upper great lakes region. *Agricultural and Forest Meteorology*, **148**, 155–157.

Cooley D, Breidt FJ, Ogle SM, Schuh AE, Lauvaux T (2012) A constrained least-squares approach to combine bottom-up and top-down CO$_2$ flux estimates. *Environmental and Ecological Statistics*, **July 04**, 1–18.

Corbin KD, Denning AS, Lokupitiya EY et al. (2010) Assessing the impact of crops on regional CO$_2$ fluxes and atmospheric concentrations. *Tellus B*, **62**, 521–532, doi: 10.1111/j.1600-0889.2010.00485.x. URL:http://dx.doi.org/10.1111/j.1600-0889.2010.00485.x.

Crosson ER (2008) A cavity ring-down analyzer for measuring atmospheric levels of methane, carbon dioxide, and water vapor. *Applied Physics B: Lasers and Optics*, **92**, 403–408, doi: 10.1007/s00340-008-3135-y.

Denning AS (2005) *Science Implementation Strategy for the North American Carbon Program*. Prepared for the U.S. Carbon Cycle Scientific Steering Group and Interagency Working Group by the North American Carbon Program Implementation Strategy Group.

Denning AS, Randall DA, Collatz GJ et al. (1996) Simulations of terrestrial carbon metabolism and atmospheric CO2 in a general circulation model. Part 2: spatial and temporal variations of atmospheric CO$_2$. *Tellus*, **48B**, 543–567.

Denning AS, Holzer M, Gurney KR et al. (1999) Three-dimensional transport and concentration of SF6: a model intercomparison study (Transcom 2). *Tellus*, **51B**, 266–297.

Denning AS, Nicholls M, Prihodko L, Baker I, Vidale PL, Davis K, Bakwin P (2003) Simulated variations in atmospheric CO$_2$ over a Wisconsin forest using a couple ecosystem-atmosphere model. *Global Change Biology*, **9**, 1241–1250.

Desai AR, Moore DJP, Ahue W et al. (2011) Seasonal pattern of regional carbon balance in the Central Rocky Mountains from the Airborne Carbon in the Mountains Experiment. *Journal of Geophysical Research-Biogeosciences*, **116**, G04009, doi: 10.1029/2011JG001655.

Dolman AJ, Noilhan J, Durand P et al. (2006) CERES, the CarboEurope Regional Experiment Strategy in Les Landes, South West France, May–June. *Bulletin of the American Meteorological Society*, **87**, 1367–1379.

Enting IG, Trudinger CM, Francey RJ (1994) A synthesis inversion of the concentration and d13C of atmospheric CO$_2$. *Tellus*, **47B**, 35–52.

EPA (2010) *Inventory of U.S. Greenhouse Gas Emissions and Sinks: 1990–2008*. U.S. Environmental Protection Agency, Washington, DC.

Evensen G (1994) Sequential data assimilation with a nonlinear quasi-geostrophic model using Monte Carlo methods to forecast error statistics. *Journal of Geophysical Research*, **99**, 143–162.

Farquhar GD, Von Caemmerer S, Berry JA (1980) A biochemical model of photosynthetic CO$_2$ fixation in the leaves of C3 species. *Planta*, **149**, 78–90.

Filippi D, Ramonet M, Ciais P, Picard D, Le Roulley JC, Schmidt M, Nedelec P (2003) Greenhouse airborne measurements over Europe. *Geophysical Reseach Abstracts*, **5**, EGS-AGU-EUG Joint Assembly, April 2003, abstract #14226.

Friedlingstein P, Cox P, Betts R et al. (2006) Climatecarbon cycle feedback analysis: results from the C4MIP model intercomparison. *Journal of Climate*, **19**, 3337–3353.

Fung I, Tucker C, Prentice K (1987) Application of advanced very high resolution radiometer vegetation index to study atmosphere-biosphere exchange of CO$_2$. *Journal of Geophysical Research*, **92**, 2999–3015.

Gerbig C, Lin JC, Wofsy SC et al. (2003) Toward constraining regional-scale fluxes of CO$_2$ with atmospheric observations over a continent: 2. analysis of cobra data using a receptor-oriented framework. Journal of Geophysical Research, 108. *ACH*, **6**, 1–19.

Goeckede M, Michalak AM, Vickers D, Turner DP, Law BE (2010a) Atmospheric inverse modeling to constrain regional scale co2 budgets at high spatial and temporal resolution. *Journal of Geophysical Research*, **115**, D15113.

Goeckede M, Turner DP, Michalak AM, Turner DP, Law BE (2010b) Sensitivity of a subregional scale atmospheric inverse CO$_2$ modeling framework to boundary conditions. *Journal of Geophysical Research*, **115**, D24112, doi:10.1029/2010JD014443.

Gourdji SM, Mueller KL, Yadav V et al. (2012) North American CO$_2$ exchange: intercomparison of modeled estimates with results from a fine-scale atmospheric inversion. *Biogeosciences Discussions*, **9**, 457–475.

Gurney KR, Law RM, Denning AS et al. (2002) Towards robust regional estimates of CO$_2$ sources and sinks using atmospheric transport models. *Nature*, **415**, 626–630.

Gurney K, Mendoza D, Zhou Y, Fischer ML, Miller CC, Geethakumar S, de la Rue du Can S (2009) High resolution fossil fuel combustion CO$_2$ emissions fluxes for the United States. *Environmental Science and Technology*, **43**, 5535–5541.

Heimann M, Keeling CD (1986) Meridional eddy diffusion model of the transport of atmospheric carbon dioxide 1. The seasonal carbon cycle over the tropical Pacific ocean. *Journal of Geophysical Research*, **91**, 7765–7781.

King AW, Dilling L, Zimmerman G et al. (2007) *Ccsp: The First State of the Carbon Cycle Report (Soccr): The North American Carbon Budget and Implications for the Global Carbon Cycle, A Report by the U.S. Climate Change Science Program and the Subcommittee on Global Change Research*. National Oceanic and Atmospheric Administration, National Climatic Data Center, Ashville, NC.

Krol M, Houweling S, Bregman B et al. (2005) The two-way nested global chemistry-transport zoom model tm5: algorithm and applications. *Atmospheric Chemistry and Physics*, **5**, 417–432.

Lauvaux T, Uliasz M, Sarrat C et al. (2008) Mesoscale inversion: first results from the ceres campaign with synthetic data. *Atmospheric Chemistry and Physics*, **8**, 3459–3471.

Lauvaux T, Pannekoucke O, Sarrat C, Chevallier F, Ciais P, Noilhan J, Rayner PJ (2009) Structure of the transport uncertainty in mesoscale inversions of CO$_2$ sources and sinks using ensemble model simulations. *Biogeosciences*, **6**, 1089–1102.

Lauvaux T, Schuh AE, Bocquet M, Wu L, Richardson S, Miles N, Davis KJ (2012a) Network design for mesoscale inversions of CO$_2$ sources and sinks. *Tellus B, North America*, **64**, 17980.

Lauvaux T, Schuh AE, Uliasz M et al. (2012b) Constraining the CO$_2$ budget of the corn belt: exploring uncertainties from the assumptions in a mesoscale inverse system. *Atmospheric Chemistry and Physics*, **12**, 337–354, doi: 10.5194/acpd-12-337-2012.

Law R, Simmonds I (1996) The sensitivity of deduced CO$_2$ sources and sinks to variations in transport and imposed surface concentrations. *Tellus*, **48B**, 613–625.

Lokupitiya R, Zupanski D, Denning AS, Kawa SR, Gurney KR, Zupanski M (2008) Estimation of global CO$_2$ fluxes at regional scale using the maximum likelihood

ensemble filter. *Journal of Geophysical Research*, **113**, D20110, doi:10.1029/2007 JD009679.

Lokupitiya E, Denning S, Paustian K *et al.* (2009) Incorporation of crop phenology in simple biosphere model (sibcrop) to improve land-atmosphere carbon exchanges from croplands. *Biogeosciences*, **6**, 969–986. URL http://www.biogeosciences.net/ 6/969/2009/.

Martins DK, Sweeney C, Stirm BH, Shepson PB (2009) Regional surface flux of CO inferred from changes in the advected CO₂ column density. *Agricultural and Forest Meteorology*, **149**, 1674–1685.

Meyers TP, Hollinger S (2004) An assessment of storage terms in the surface energy balance of maize and soybean. *Agricultural and Forest Meteorology*, **125**, 105–115, doi: http://dx.doi.org/10.1016/j.agrformet.2004.03.001.

Michalak AM, Bruhwiler L, Tans PP (2004) A geostatistical approach to surface flux estimation of atmospheric trace gases. *Journal of Geophysical Research*, **109**, 1–19.

Miles NL, Richardson SJ, Davis KJ *et al.* (2012) Large amplitude spatial and temporal gradients in atmospheric boundary layer CO₂ mole fractions detected with a tower-based network in the U.S. upper midwest. *Journal of Geophysical Research Biogeosciences*, **117**, G01019.

Nicholls ME, Denning AS, Prihodko L, Vidale PL, Baker IT, Davis K, Bakwin P (2004) A multiple-scale simulation of variations in atmospheric carbon dioxide using a coupled biosphere-atmospheric model. *Journal of Geophysical Research*, **109**, D18117, 10.1029/2003JD004482.

Ogle S, Davis K, Andrews A *et al.* (2006) *Science Plan: Mid-CONTINENT Intensive Campaign of the North American Carbon Program*. North American Carbon Program, Greenbelt, MD.

Ogle S, Breidt F, Easter M, Williams S, Killian K, Paustian K (2010) Scale and uncertainty in modeled soil organic carbon stock changes for us croplands using a process-based model. *Global Change Biology*, **16**, 810–820.

Olsen S, Randerson J (2004) Differences between surface and column atmospheric CO₂ and implications for carbon cycle research. *Journal of Geophysical Research*, **109**, D02301, doi: 10.1029/2003JD003968.

Pearman G, Hyson P (1981) The annual variation of atmospheric CO₂ concentration observed in the northern hemisphere. *Journal of Geophysical Research*, **86**, 9839–9843.

Peters W, Jacobson AR, Sweeney C *et al.* (2007) An atmospheric perspective on North American carbon dioxide exchange: Carbontracker. *Proceedings of the National Academy of Sciences of the United States of America*, **104**, 18925–18930.

Peters W, Krol M, Van Der Werf GR *et al.* (2010) Seven years of recent European net terrestrial carbon dioxide exchange constrained by atmospheric observations. *Global Change Biology*, **16**, 1317–1337.

Pielke RA, Cotton W, Walko R *et al.* (1992) A comprehensive meteorological modeling system – rams. *Meteorology and Atmospheric Physics*, **46**, 69–91.

Richardson SJ, Miles NL, Davis KJ *et al.* (2012) Field testing of cavity ring-down spectroscopy analyzers measuring carbon dioxide and water vapor. *Journal of Atmospheric and Oceanic Technology*, **29**, 397–406.

Schuh AE, Denning AS, Uliasz M, Corbin KD (2009) Seeing the forest through the trees: recovering largescale carbon flux biases in the midst of smallscale variability. *Journal of Geophysical Research*, **114**, G03007, doi: 10.1029/2008JG000842.

Schuh AE, Denning AS, Corbin KD, Dalcher A (2010) A regional high-resolution carbon flux inversion of North America for 2004. *Biogeosciences*, **8**, 1625–1644.

Sellers PJ, Mintz Y, Sud YC, Dalcher A (1986) A simple biosphere model (sib) for use within general circulation models. *Journal of Atmospheric Sciences*, **43**, 505–531.

Sellers PJ, Randall DA, Collatz GJ *et al.* (1996) A revised land surface parameterization (sib2) for atmospheric gcms. part i: model formulation. *Journal of Climate*, **9**, 676–705.

Skamarock WC, Klemp JB, Dudhia J, Gill DO, Barker DM, Wang W, Powers JG (2005) *A Description of the Advanced Research WRF Version 2*. National Center of Atmospheric Research, Boulder, CO.

Solomon S, Qin D, Manning M *et al.*, eds. (2007) *IPCC, 2007: Climate Change 2007: The Physical Science Basis. Contribution of Working Group I to the Fourth Assessment Report of the Intergovernmental Panel on Climate Change*. Cambridge University Press, Cambridge, UK and New York, NY.

Stephens BB, Miles NL, Richardson SJ, Watt AS, Davis KJ (2011) Atmospheric CO₂ monitoring with single-cell ndir-based analyzers. *Atmospheric Measurement Techniques*, **4**, 2737–2748.

Tans PP, Fung IY, Takahashi T (1990) Observational constraints on the global atmospheric CO₂ budget. *Science*, **247**, 1431–1438.

Tarantola A (1987) *Inverse Problem Theory: Methods for Data Fitting and Parameter Estimation*. Elsevier Science, New York.

Tippett M, Anderson JL, Bishop CH, Hamill T, Whitaker J (2003) Ensemble square-root filters. *Monthly Weather Review*, **131**, 1485–1490.

Uliasz M (1993) The atmospheric mesoscale dispersion modeling system (mdms). *Journal of Applied Meteorology*, **32**, 139–149.

Uliasz M (1994) Lagrangian particle modeling in mesoscale applications. In: *Environmental Modeling II* (ed. Zannetti P), pp. 71–102. Computational Mechanics Publications, Southampton, UK.

Uliasz M (1996) Lagrangian particle modeling in mesoscale applications. In: *Environmental Modeling III* (ed. Zannetti P), pp. 145–182. Computational Mechanics Publications, Southampton, UK.

Uliasz M, Pielke RA (1991) Application of the receptor oriented approach in mesoscale dispersion modeling. In: *Air Pollution Modeling and its Applications VIII* (eds Dop HV, Steyn DG), pp. 399–408. Plenum Press, New York.

Verma S, Dobermann A, Cassman K *et al.* (2005) Annual carbon dioxide exchange in irrigated and rainfed maize-based agroecosystems. *Agricultural and Forest Meteorology*, **131**, 77–96.

Wang JW, Denning AS, Lu L, Baker IT, Corbin KD, Davis KJ (2006) Observations and simulations of synoptic, regional, and local variations in atmospheric CO₂. *Journal of Geophysical Research*, **112**, D04108, doi: 10.1029/2006JD007410.

van der Werf G, Randerson JT, Giglio L, Collatz GJ, Kasibhatia PS, Arellano . AF Jr (2006) Interannual variability in global biomass burning emissions from 1997 to 2004. *Atmospheric Chemistry and Physics*, **6**, 3423–3441, doi: 10.5194/acp-6-3423-2006.

West TO, Bandaru V, Brandt CC, Schuh AE, Ogle SM (2011) Regional uptake and release of crop carbon in the United States. *Biogeosciences*, **8**, 2037–2046.

Whitaker JS, Hamill TM (2002) Ensemble data assimilation without perturbed observations. *Monthly Weather Review*, **130**, 1913–1924.

Wofsy SC, Harriss RC (2002) The North American Carbon Program plan (NACP): a report of the Committee of the U.S. Carbon Cycle Science Steering Group. Prepared at the Request of the Agencies of the U.S. Global Change Research Program.

Wu L, Bocquet M, Lauvaux T, Chevallier F, Rayner P, Davis KJ (2011) Optimal representation of source–sink fluxes for mesoscale carbon dioxide inversion with synthetic data. *Journal of Geophysical Research*, **116**, D21304, doi: 10.1029/2011JD016198.

Zupanski M (2005) Maximum likelihood ensemble filter. Thoretical aspects. *Monthly Weather Review*, **133**, 1710–1726.

Zupanski D, Denning AS, Uliasz M *et al.* (2007) Carbon flux bias estimation employing maximum likelihood ensemble filter (mlef). *Journal of Geophysical Research*, **112**, D17107, doi: 10.1029/2006JD008371.

Supporting Information

Additional Supporting Information may be found in the online version of this article:

Data S1. Appendices.

Figure A1. Inversion domains shown in native polar stereographic projections. Left panel (A) shows nested inversion grid with coarser grid at 200 km by 200 km and fine grid over MCI at 40 km by 40 km. Right panel (B) shows high resolution 20 km by 20 km grid for PSU inversion system.

Figure A2. CarbonTracker ecoregion-based inversion domain. Figure courtesy of NOAA-ESRL.

Figure C1. Time series of net ecosystem exchange (NEE) estimates from a variety of inversion models for 2007. PSU inversion is based on SiB3-CROP offline prior. CSU inversion is also based on SiB3-CROP offline prior with GV-bias corrected-CT inflow. Results from PSU inversion are from the intersection of PSU inversion domain and MCI domain while the results for the Carbon-Tracker and CSU inversions are on the MCI domain.

Figure D1. Sensitivity of daytime observations of passive surface flux to daytime passive flux releases during June, July, and August. Left panel shows results for PSU transport with WRF and LPDM and middle panel shows results for CSU transport with RAMS and LPDM. Right panel shows the difference. Releases were constant 1 μmol C m^{-2} s^{-1} over the PSU inversion domain (subset of MCI) and passive signal was integrated over this same area for both models.

Figure D2. Sensitivity of daytime observations of passive surface flux to nighttime passive flux releases during June, July, and August. Left panel shows results for PSU transport with WRF and LPDM and middle panel shows results for CSU transport with RAMS and LPDM. Right panel shows the difference. Releases were constant 1 μmol C m^{-2} s^{-1} over the PSU inversion domain (subset of MCI) and passive signal was integrated over this same area for both models.